18th Brazilian Congress of Thermal Sciences and Engineering
November 16-20, 2020 (Online)

ENC-2020-0424
EXPERIMENTAL AND NUMERICAL INVESTIGATION OF THE FLOW IN SLIDING SLEEVE VALVES

Suellen Freire Rigatto da Cruz
Rodrigo Mageski Tavares
Rodrigo Simões Maciel
Lucas Zampirole Brandão
Fabio de Assis Ressel Pereira
Bruno Venturini Loureiro
Federal University of Espirito Santo, Vitória/ES, 29075-910, Espirito Santo, Brazil
suellenfrigatto@gmail.com
mageski.rodrigo@gmail.com
rodrigosimoesrsm@gmail.com
lucaszb22@gmail.com
fabio.a.pereira@ufes.br
bruno.loureiro@ufes.br

Andre Leibsohn Martins
Petrobras, Rua Horacio Macedo, 950, Rio de Janeiro/RJ, 21941-915, Rio de Janeiro, Brazil
aleibsohn@petrobras.com.br

Abstract. *In the present study it's analyzed numerically, with support of Ansys Fluent software, water flow in a three-dimensional geometry, which in a simplified way, represented a Sliding Sleeve valve. Polyhedral and tetrahedral mesh was used to compare results, and polyhedral mesh presented better results than tetrahedral mesh. The numerical results were validated with results obtained experimentally, using the Particle Image Velocimetry (PIV) technique. The results show that the numerical modeling performed adequately represents the problem.*

Keywords: *Sliding Sleeve valve, Ansys Fluent, PIV, tetrahedral mesh, polyhedral mesh*

1. INTRODUCTION

The deepwater oil production process is associated with high financial costs and all essential costs to reduce well construction costs and mitigate the risks of production losses, seeking, in the stage of completing an oil well, an optimization of the production flow in order to make the conclusion as permanent as possible, minimizing the need for intervention in the well. And, due to the fact that smart well completion technology is normally used in the Brazilian pre-salt areas, Sliding Sleeve valves, considered a new technology and which has gained importance in the oil and gas industry, represent a category Inflow Control Valves (ICV), have a significant role in the completion stage, being important their perfect functioning within their pre-established working conditions (Thomas, 2004; Correia et al., 2017; Joubran, 2018; Martins et al, 2020).

Based on the relevance attributed to smart well completion technology, the present study aims to model, using CFD techniques to be compared with experimental data, the flow in a Sliding Sleeve valve.

2. BIBLIOGRAPHIC REVIEW

2.1 Sliding Sleeve valves

The increased complexity of the reservoir and production in subsea fields results in a growing demand for the use of intelligent completion in wells, such as the ICV (Guan et al., 2018).

Some authors, among which can be cited Joubran (2018); Guan et al. (2018); Bouamra et al. (2019) and Maciel et al. (2019), evaluate, using Computational Fluid Dynamics (CFD) techniques, ICVs used in the oil well completion process. The results obtained by these authors point to the feasibility of using CFD techniques for the representation of fluid dynamics in well completion equipment.

Joubran (2018) discusses, in his study, the significant technological advances and reliability related to ICVs. According to the author, it has been searched for more reliable intelligent completion systems and rich in resources that have controls, installation and long service life procedures. In addition, significant improvements in ICV reliability have been made with useful and practical resources.

There is a growing demand for the use of intelligent completion in wells, such as ICV, due to the increased complexity of the reservoir and production in subsea fields, and the work developed by Guan et al. (2018) evaluate numerically the risks of the fouling phenomenon occurring over the life of the field for a carbonate reservoir in the pre-salt, with a much greater fouling potential identified in the ICV region. In particular, Guan et al. (2018) show the importance of using fouling simulation tools to assist in the selection of laboratory test conditions; applying CFD modeling to guide the design of high-value test equipment and to reveal the mechanisms.

Due to the importance attributed to ICVs, the most appropriate modeling should be sought to represent the flow in them. In this scenario, the present study analyzes the fluid dynamics in a Sliding Sleeve valve. Using an experimental study of this same valve, it is possible to verify the adequacy of the numerical modeling of the flow in the valve, taking into account the computational cost and the error presented in relation to the experimental result.

The study has as general objective to validate the numerical modeling in a Sliding Sleeve valve; and as specific objectives, to highlight the advantages of using polyhedral meshes and to analyze the influence of the use of tetrahedral and polyhedral meshes in Sliding Sleeve valves.

2.2 Particle Image Velocimetry - PIV

The PIV technique for measuring instantaneous velocity fields is based on determining the displacement field of tracer particles previously distributed in the fluid in a given time interval. The time for evaluation of displacement of particles must be short when compared to smaller time scales characteristic of the flow, so that the measured displacement field can be considered as being instantaneous. The velocity field is obtained from the ratio between displacement and time.

The general principle of operation of PIV technique can be better understood with the aid of Fig 1. In the figure, schematically, a flow of fluid containing tracer particles through a rectangular section duct is shown. A light plane is formed with a beam from a pulsed laser source. A set of lenses is used to form the plane from a laser beam. The light plane hits the flow section illuminating tracer particles present in the region of the illuminated plane (Raffel et al., 2018).

A camera is positioned orthogonal to the lighting plane. The capture of images of particles is synchronized with pulses of the laser, whose time interval is known and precisely determined by the electronic equipment that controls the laser source. In this way, two consecutive images of particles are obtained passing in the illuminated plane.

The velocities of tracer particles are obtained from their displacements measured in captured images and interval between pulses used.

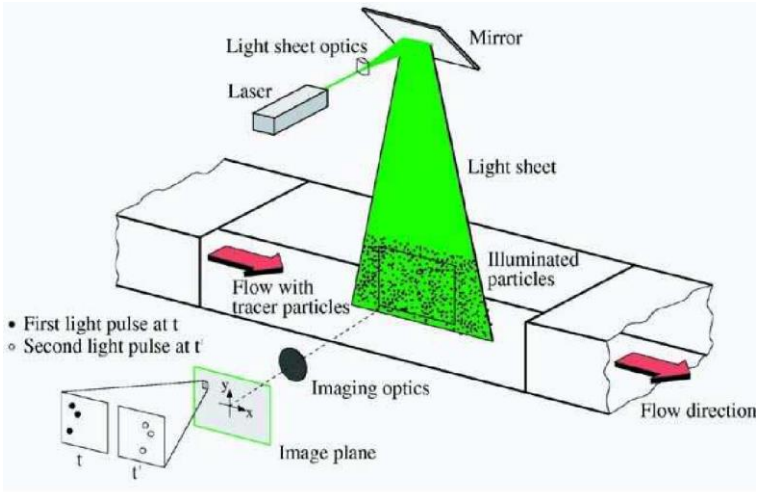

Figure 1. Illustration of the PIV technique. Available from: Raffel et al. (2018).

2.3 Polyhedral and tetrahedral mesh

According to Sosnowski (2017), in fluid dynamics it is desirable that the domain is discretized into hexahedral elements characterized by low numerical diffusion, particularly in the case of flow perpendicular to the faces of the control volumes. However, structured hexahedral meshes are not viable for complex geometries, which can be modeled by tetrahedral and polyhedral meshes. Thus, tetrahedral meshes are an option because the element is formed by four faces and is simpler compared to other elements. The main advantage of tetrahedral meshes is the ease of generating meshes

even in complex geometries. However, tetrahedral elements cannot elongate too much, causing an excessive number of elements compared to hexahedral meshes.

The polyhedral mesh was created with the objective of combining the advantages of hexahedral and tetrahedral meshes, that is, low numerical diffusion and fast semi-automatic generation, respectively. The main advantage of polyhedral meshes is the fact that each element has several neighbors, so that gradients can be calculated more accurately in comparison to tetrahedral mesh. In addition, polyhedral elements are less sensitive to stretching, making the model with greater numerical stability (Sosnowski, 2017).

3. MATHEMATICAL MODELING

3.1 Mass's conservation and momentum

Through a numerical discretization approach, equations of mass's conservation and momentum are solved for each discrete element of the control volume, which form the computational domain (Maciel et al., 2019). Mass conservation and the conservation of the momentum, can be described according to Eq. (1) and Eq. (2), respectively (Ansys, 2019).

$$\frac{\partial \rho}{\partial t} + \nabla \cdot \left(\rho \vec{V}\right) = S_m \tag{1}$$

$$\frac{\partial}{\partial t}(\rho \vec{v}) + \nabla \cdot (\rho \vec{v} \vec{v}) = -\nabla P + \nabla \cdot (\bar{\bar{\tau}}) + \rho \vec{g} + \vec{F} \tag{2}$$

Where S_m represents a possible source of mass within the domain (for example, chemical reaction, vaporization of phases, etc.) and becomes zero when there is no source. The term P corresponds to the static pressure and $\bar{\bar{\tau}}$ the stress tensor, Eq. (3). The terms $\rho \vec{g}$ and $\vec{F}$ represent the gravitational and body forces, respectively (Ansys, 2019).

$$\bar{\bar{\tau}} = \mu \left[(\nabla \vec{v} + \nabla \vec{v}^T) - \frac{2}{3} \nabla \cdot \vec{v} I \right] \tag{3}$$

The term μ corresponds to molecular viscosity, I is the identity matrix and the second term of the right side of the equality represents the effects of volumetric expansion.

3.2 Law of the wall

For turbulent flows of Newtonian fluids in a pipeline, a dimensionless analysis can present a clear idea about the shape of the average velocity profile in the region close to the wall (Tennekes and Lumley, 2018). For this, it is convenient to represent the average dimensionless velocity profile in y+ wall coordinates and with velocities normalized by the friction speed, μ_t. The wall coordinates are defined by Eq. (4) and Eq. (5).

$$u^+ = \frac{u}{u_t} \tag{4}$$

$$y^+ = \frac{y u_t}{v} \tag{5}$$

With $u_t = \sqrt{\frac{f V^2}{8}}$. Where f is the friction factor and V is the mean flow velocity.

3.3 Turbulence modeling

The realizable k-ε model is one of the most common turbulence models. Two equations are used, one transport equation to represent a turbulent viscosity and another to represent a turbulent dissipation rate. The realizable term means that the model satisfies mathematical constraints on Reynolds stresses consistent with turbulent flow physics (Ansys, 2019).

According to Ansys (2019), the transport equations for turbulent kinetic energy k and their dissipation rate ε in the realizable k-ε model are presented by Eq. (6) and (7).

$$\frac{\partial}{\partial t}(\rho k) + \frac{\partial}{\partial x_i}(p k u_i) = \frac{\partial}{\partial x_j}\left[\left(\mu + \frac{\mu_t}{\sigma_k}\right)\frac{\partial k}{\partial x_j}\right] + G_k + G_b - \rho\varepsilon - Y_M + S_K \tag{6}$$

$$\frac{\partial}{\partial t}(\rho \varepsilon) + \frac{\partial}{\partial x_i}(p \varepsilon u_i) = \frac{\partial}{\partial x_j}\left[\left(\mu + \frac{\mu_t}{\sigma_\varepsilon}\right)\frac{\partial \varepsilon}{\partial x_j}\right] + C_{1\varepsilon}\frac{\varepsilon}{k}(G_k + C_{3\varepsilon}G_b) - C_{2\varepsilon}\rho\frac{\varepsilon^2}{k} + S_\varepsilon \tag{7}$$

Where G_k represents the generations of turbulent kinetic energy due to the average velocity gradient. G_b is the generation of turbulent kinetic energy due to buoyancy. Y_M represents the effects of fluctuation in the volumetric expansion for compressible turbulent flows in the total of the dissipation rate. σ_k and σ_ε represents, respectively, the turbulent Prandtl numbers for k and ε. S_K and S_ε are user-defined source terms. The terms $C_{1\varepsilon}$ and $C_{2\varepsilon}$ are constants.

The turbulent viscosity μ_t is defined by Eq. (8).

$$\mu_t = \rho C_\mu \frac{k^2}{\varepsilon} \tag{8}$$

Since C_μ is obtained by Eq. (9),

$$C_\mu = \frac{1}{A_0 + A_S \frac{kU^*}{\varepsilon}} \tag{9}$$

Where $U^* = \sqrt{S_{ij}S_{ij} + \widetilde{\Omega}_{ij}\widetilde{\Omega}_{ij}}$ and $\widetilde{\Omega}_{ij} = \overline{\Omega_{ij}} - \varepsilon_{ijk}\omega_k - 2\varepsilon_{ijk}\omega_k$. The term $\overline{\Omega_{ij}}$ represents the average rate of rotation tensor observed in a reference rotational angular velocity. The constants A_0 and A_S are: $A_0 = 4.04$ and $A_S = \sqrt{6}\cos\phi$. Where $\phi = \frac{1}{3}\cos^{-1}\left[\sqrt{6}\frac{S_{ij}S_{jk}S_{ki}}{\tilde{s}^3}\right]$, $\tilde{s} = \sqrt{S_{ij}S_{ij}}$ and $S_{ij} = \frac{1}{2}\left[\frac{\partial u_j}{\partial x_i} + \frac{\partial u_i}{\partial x_j}\right]$.

4. METHODOLOGY

4.1 Experimental investigation

The project of the valve for the experimental case, Fig. 2, was printed with 0.03 mm resolution, using a 3D printer STRATASYS OBJET30 PRO.

Figure 2. Illustration of the valve for the experimental case.

The experimental bench consists of a closed circuit where the components are shown in the sketch in Fig. 3. To start the test, first place the sliding sleeve valve (VII) inside the borosilicate glass tube, so that the trim is orthogonal to the laser and the camera (VI). Subsequently, this tube is fixed in the viewing box (V) and it is placed on the bench and then checked if the tube is perpendicular to the camera.

After assembling the bench, the mixer is filled with 50 kg of filtered water (I). With pump on, 15 ppm of glass particles are added, which are dispersed by means of a magnetic mixer that promotes a constant rotation of the sample.

The solution is then sucked up by the pump (II), which directs the fluid to the test section where the flow and static pressure difference are measured by means of an electromagnetic meter (III) and pressure taps (IV), respectively. After that, the solution returns to the tank.

In the trim region, the particle image velocimetry system is used to acquire and evaluate velocity profiles along the valve.

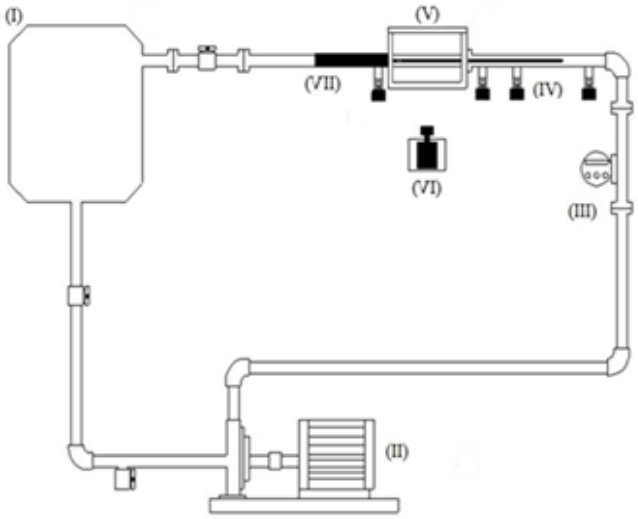

Figure 3. Sketch of experimental apparatus, consisting of (I) mixer, (II) centrifugal pump, (III) flowmeter, (IV) pressure taps, (V) acrylic box, (VI) camera and (VII) sliding sleeve valve.

It is essential, for a good acquisition, the perpendicularity between camera and laser plane, as well as the alignment of the trim with these.

To obtain the average velocity fields are acquired five thousand frames of the flow in the trim region. With that, we will have two and a half thousand instantaneous velocity fields, from which the average velocity field is calculated. This large number of photos is necessary to ensure good sampling, especially if turbulent flow properties are studied.

4.2 Numerical investigation

In the present work, the results obtained experimentally, with the aid of the Particle Image Velocimetry (PIV) technique, called experimental case, are compared with two numerical cases, modeled using the Ansys Fluent software, tetrahedral case and polyhedral case, composed, respectively, by tetrahedral and polyhedral meshes. The simplified geometry of the valve is shown in Fig. 4, where the region of interest in this study is referred to as the trim and is highlighted with a red rectangle. To analyze this region, a plane is constructed on the YZ axis by axially cutting the highlighted trim with a red rectangle. Figure 5(a) and 5(b) show, respectively, the tetrahedral mesh and the polyhedral mesh, seen from the trim region, highlighted by the red rectangle in Fig. 4(a) and 4(b).

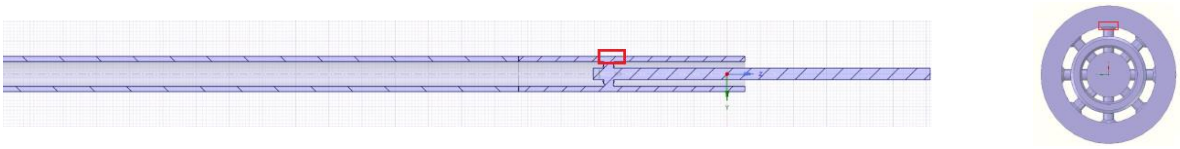

(a) YZ view (b) XY view

Figure 4. Axial section of the simplified geometry of the Sliding Sleeve valve with the trim region highlighted.

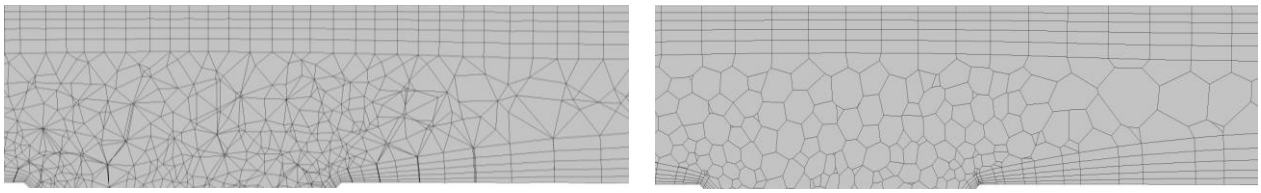

(a) Tetrahedral case (b) Polyhedral case

Figure 5. (a) Tetrahedral mesh and (b) Polyhedral mesh at the trim region.

The numerical cases use the realizable k-ε turbulence model and the meshes of the tetrahedral and polyhedral cases are formed, respectively, by 1.26 and 0.691 million of elements. As initial and boundary conditions, for both cases, the velocity of the working fluid, which is water, is 0.93 m/s at the entrance, geometry annular region; in the outlet, the gauge pressure is zero; the walls are stationary; the effects of gravitational forces are considered in geometry; the pressure variation along the valve is specified by pressure taps installed along the experimental bench installed in the laboratory of the Federal University of Espírito Santo (Ufes).

The flow rate is 0.629 m³/h and the Reynolds in the annular region is 18,000. The geometry has two roughness values, in the gray region the roughness is 7.1 μm, while in the orange region it is 5.4 μm, Fig 6. The computational flow time considered is 10 seconds and the convergence criterion is 10^{-3}.

Figure 6. YZ view of Sliding Sleeve valve geometry.

The proper choice of discretization methods represents an important step in the simulation process, this choice being made in order to achieve the convergence of the simulated results.

The solution scheme of the equations was pressure-based. For pressure-velocity coupling the SIMPLE (Semi-Implicit Method for Pressure Linked Equations) algorithm was employed. To evaluate the gradients of conserved properties, the Least Squares Cell-Based method was applied. The pressure interpolation scheme was Standard. For the momentum, turbulent kinetic energy and turbulent dissipation rate the scheme used was the First Order Upwind. For the transient formulation, the First Order Implicit procedure was adopted. In order to get best results near the wall, Standard Wall Treatment was applied. This approach has been most widely used in industrial flows (Ansys, 2019).

5. RESULTS/DISCUSSION

5.1 Analysis of turbulence in geometry

The non-dimensional wall distance y+ (YPlus) is used for the determination of turbulent flows delimited by walls. According to Salim and Cheah, (2009), the y+ that best represents the viscous sublayer is found in y+<5 and for an adequate representation of the Log Law region the y+ should be between 30 and 60. For the k-ε turbulence model, a y+≈30 is already sufficient, because in this case, wall functions were used (Salim and Cheah, 2009). Figure 7 shows the parameter y+ in the region close to the trim entrances.

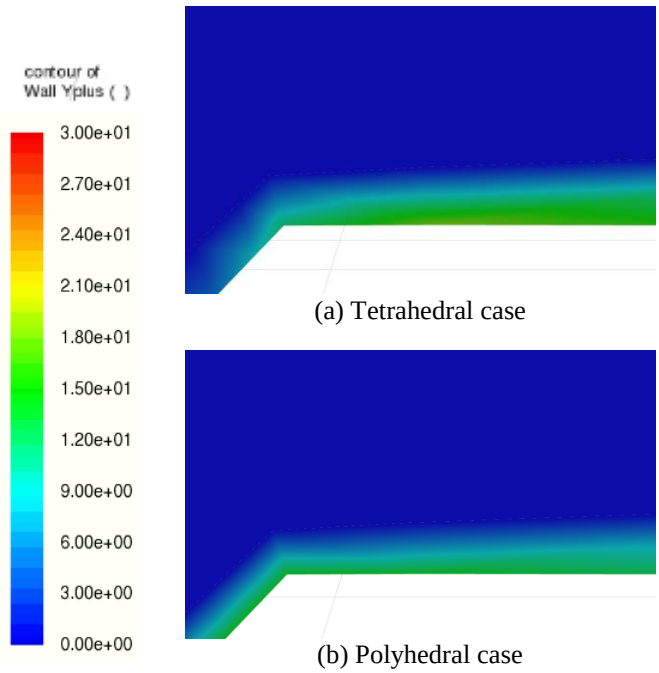

(a) Tetrahedral case

(b) Polyhedral case

Figure 7. Y+ contours in the region close to the trim entrances.

It can be seen, in Fig. 7, that the maximum value of y+, in the region close to the trim entrances, was approximately 18 for both cases, indicating, for the both meshes used, an appropriate representation of the turbulence model used with respect to the representation of the turbulent boundary layer.

5.2 Analysis of velocity in geometry

The velocity contours for the tetrahedral, polyhedral and experimental cases are shown, respectively, in Fig. 8(a), Fig. 8(b) and Fig. 8(c). The velocity vectors in Fig. 8(c) were calculated with the experimental data obtained by the PIV technique, which presents, in a 2D image, an average velocity at all times throughout the experimental process. Fig. 8(a) e Fig. 8(b) are obtained from a plane, in 3D geometry, that is constructed on the YZ axis by axially cutting the trim.

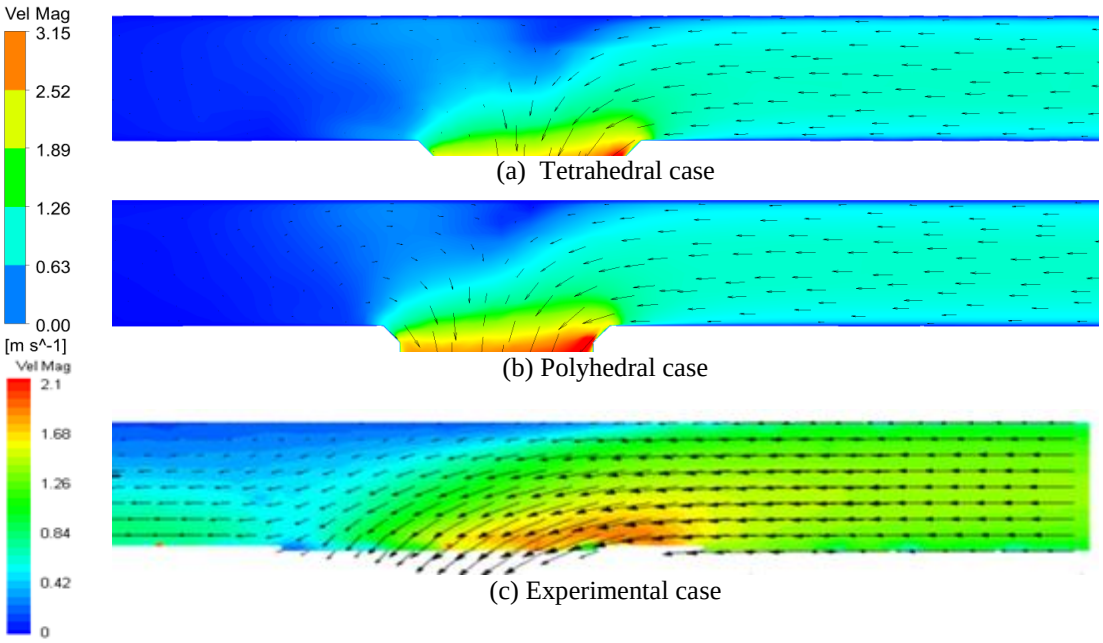

(a) Tetrahedral case

(b) Polyhedral case

(c) Experimental case

Figure 8. Velocity contours at the trim entrance.

As noted in Fig. 8, there are no significant divergences between the velocity contours in the region close to the trim entrances, both in the tetrahedral and polyhedral cases, when compared to the experimental case, indicating an adequate agreement between the experimental and numerical results. Therefore, choosing the most appropriate mesh for modeling the phenomenon presented in this report should take into consideration other parameters such as the pressure variation along the geometry and the defendant computational time.

A recirculation zone can also be observed, at the left end, in all numerical cases, Fig. 8(a) and Fig. 8(b). However, this recirculation zone is not observed in the experimental case, Fig. 8(c). Therefore, the streamlines are helpful to the better understanding of the fluid flow phenomenon in the geometry for the numerical cases, Fig. 9(a) and Fig. 9(b).

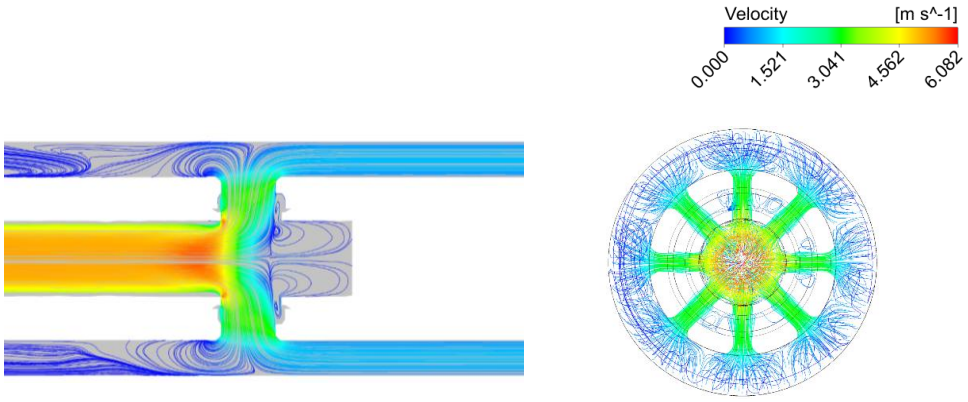

(a) YZ view (b) XY view

Figure 9. Velocity streamlines in the geometry for the numerical cases.

The streamlines, Fig. 9(a) and 9(b), show that there is a recirculation zone near the trim entrance. This phenomenon could be a result of influence of adjacent trim, as shown in Fig 9(b).

Regarding the computational time, the polyhedral case requires approximately 30,600 seconds to reach 10 seconds of flow. While the tetrahedral case requires approximately 72,000 seconds to reach the same flow time. Thus, it can be seen that the polyhedral mesh achieved similar results with a computational time 57.5% less than the tetrahedral mesh.

To validate the numerical model, the pressure variation along the valve is analyzed, calculated between the two differential pressure taps installed next to the valve. The experimental case presents a pressure variation along the valve of 32.4 kPa, while the polyhedral case presents a variation of 30.5 kPa, and the tetrahedral case presents 26.0 kPa. The fact that the polyhedral Case presents only a pressure variation of 5.86% smaller than the experimental result points out the compatibility of the numerical modeling with the experimental data for the adequate representation of the problem.

The difference between the two cases using the k-ε turbulence model, polyhedral case and tetrahedral case, is the type of mesh element, and the result shows that the polyhedral mesh, was the one that reached a result of pressure variation more close to the experimental case, in relation to the tetrahedral case, this phenomenon resulting from the advantages of the polyhedral mesh over the tetrahedral mesh.

6. CONCLUSION

In the numeric cases the values of velocity of the trim entrance are near to the values found in the experimental test. Furthermore, the tetrahedral case presented 8.42% of difference to the experimental case, and the polyhedral case presented a difference of 5.86% in the pressure variation, if compared with experimental results, indicating a better performance of the polyhedral mesh compared to the tetrahedral mesh, since it presented a shorter computational time and was closer to the experimental results.

In addition, using the PIV technique, a recirculation region close to the trim, in the upper region, was observed due to the change in direction of the flow. This change in direction is caused by the trim. It is also observed, immediately after the trim and in the lower region, a field with a relatively high velocity, this is due to the fact that the trim is interspersed, that is, the fluid is flowing to the trim downstream of this observed. However, as the obtained velocity field is two-dimensional, with the axial and radial components, only these two components are represented in the results, giving the impression that the flow occurs only in the axial direction when passing through the trim.

7. ACKNOWLEDGEMENTS

The authors would like to thank Petrobras to financially support this research.

8. REFERENCES

Ansys, 2019. “Fluent Theory Guide”.

Bouamra, R., Carneiro, G., Machado, P., Silva, M.F., Franquiz, G., Guan, H. and Lindvig, T., 2019. “ScaleProTect–Scale Deposition Modeling in Pre-Salt Reservoir”. In *Offshore Technology Conference Brasil*.

Correa, N.A., Barcelos, T.F.P., Miura, K., Mendes, J.R.P., 2017. “Intelligent Completion or Well Intervention Robot?”. In *Abu Dhabi International Petroleum Exhibition & Conference.* Society of Petroleum Engineers.

Guan, H., Bouamra, R., Lindvig, T. and Vernus, J. C., 2018. "Scale Risk Assessment and Novel Coating for Smart Completion: Scale Simulation and CFD Modelling Approach". In *SPE International Oilfield Scale Conference and Exhibition*. Society of Petroleum Engineers.

Joubran, J., 2018. "Intelligent Completions: Design and Reliability of Interval Control Valves in the Past, Present, and Future". In *Offshore Technology Conference*.

Maciel, R.S., Pereira, F.R.A., Fejoli, R.F., Martins, A.L. and Ferreira, M.V.D., 2019. "Enhancing Scale Prediction in Pre-Salt Wells Using Numerical Simulation". In *SPE Annual Technical Conference and Exhibition. Society of Petroleum Engineers*.

Martins, A.L., Castro, B.B., Schluter, H.E.P., Ferreira, M.V.D., Achy, A.R.A. and Pepe, I.M., 2020. "Offshore Field Experience with Non Chemical Oilfield Scale Prevention/Remediation Strategies in Brazil". In *Offshore Technology Conference*.

Raffel, M., Willert, C.E., Scarano, F., Kähler, C.J., Wereley, S.T. and Kompenhans, J., 2018. "Particle image velocimetry: a practical guide". *Springer*.

Salim, S. M. and Cheah, S. "Wall Y strategy for dealing with wall-bounded turbulent flows". 2009. In *Proceedings of the International Multiconference of Engineers and Computer Scientists*. Vol. 2, pp. 2165-2170.

Sosnowski, M., Krzywanski, J., Gnatowska, R., 2017. "Polyhedral meshing as an innovative approach to computational domain discretization of a cyclone in a fluidized bed CLC unit". E3S Web of Conferences 14, [s. l.]. DOI 10.1051/ 71401027.

Tennekes, H. and Lumley, J. L., 2018. "A first course in turbulence". *MIT press.*

Thomas, J.E. (Org.)., 2004. "Fundamentos de Engenharia de Petróleo". Rio de Janeiro: *Interciência*. Petrobras.

9. RESPONSIBILITY NOTICE

The authors are the only responsible for the printed material included in this paper.